THE JOURNAL OF PHYSICAL CHEMISTRY C

Article

Cite This: J. Phys. Chem. C 2018, 122, 20632−20641

pubs.acs.org/JPCC

Molecular Probes Reveal Chemical Selectivity of the Solid−Electrolyte Interphase

Oliver C. Harris and Maureen H. Tang*

Chemical & Biological Engineering, Drexel University, 3141 Chestnut Street, Philadelphia, Pennsylvania 19104, United States

Supporting Information

ABSTRACT: The solid−electrolyte interphase (SEI) is well-known to provide critical protection between the strongly reducing negative electrode and the organic electrolytes of nonaqueous batteries. Batteries with a poorly passivating SEI will suffer from rapid capacity fade and short lifetimes. Despite its importance and extensive study of its structure and composition, the mechanism of SEI passivation remains poorly understood. In this work, we demonstrate using electrochemical collector-generator measurements that the SEI is chemically selective in its passivation and propose a model based on catalytic active sites to explain its performance. Electrochemically interrogating the SEI with functionalized ferrocene mediators shows that the through-film mediator reduction is much more sensitive to mediator functional group than size, indicating preferential partitioning into the organic SEI layer. Additional experiments with controlled electrode crosstalk show that incorporation of dissolved transition metals increases both the density and the activity of active sites within the SEI. We conclude that the inner, inorganic layer is responsible for preventing charge transfer through the SEI while the outer, organic layer is minimally important. Our model reconciles contradictory observations from the literature and identifies the most important components of a functional battery interface.

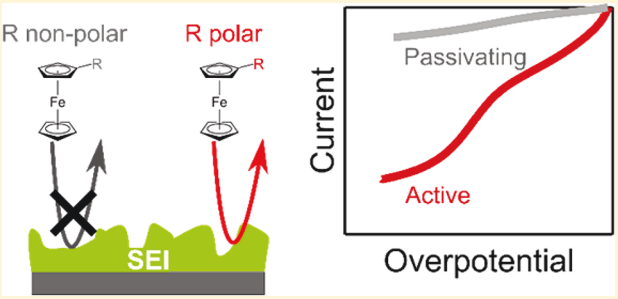

Downloaded via DREXEL UNIV on September 20, 2018 at 15:12:26 (UTC).
See https://pubs.acs.org/sharingguidelines for options on how to legitimately share published articles.

INTRODUCTION

The solid−electrolyte interphase (SEI) is vital to the lifetime of Li-ion and other advanced battery chemistries. Consumption of cyclable Li during its formation and growth remains the leading cause of capacity fade in Li-ion batteries, yet the underlying mechanism of how the film fails or succeeds to protect the battery remains elusive. Since its discovery in 1979, the film has been studied extensively.[1−3] SEI composition and performance vary based on the anode material, electrolyte composition, and even the cathode material due to electrode crosstalk.[4]

In particular, electrode crosstalk accelerates SEI growth and capacity fade in high-voltage batteries, resulting in unacceptably poor battery lifetimes.[5−10] This accelerated capacity fade is due to dissolution of metals from the transition metal oxide cathode.[11] At voltages above 4.2 V vs Li/Li$^+$, transition metals dissolve out of the cathode active material[12,13] and travel to the anode, where they interfere with SEI reactions and cause rapid capacity fade. Mn and Ni have been detected at the negative electrode as deposits and in the bulk electrolyte.[4,10,12,14−17] Abraham et al. have shown that dissolved Mn, rather than other metals, is the leading contributor to accelerated capacity fade; thus, the role of Mn has been the topic of extensive research over the past decade.[13]

While researchers agree that Mn contamination of the SEI is responsible for short battery lifetimes, there is little agreement over the effects of Mn on the mechanisms of passivation, the location of Mn within the SEI, and the oxidation state of the dissolved species. One school of thought is that metal deposition within the SEI forms a conductive pathway for electrons to easily hop to an electrolyte molecule,[14,18] while another school maintains that Mn catalyzes gas-evolving reactions that cause the SEI to crack and allow facile electrolyte transport.[10,18,19] A third explanation hypothesizes that deposited Mn reduces electrolyte molecules via a catalytic cycle.[13,20−22]

Confusion over the role of Mn in SEI disruption points to a deeper, unresolved question: namely, how does the SEI block charge transfer, even without Mn contamination? It is accepted that a protective SEI is electronically insulating yet Li-ion conducting.[2] Additionally, multiple reports have observed a bilayer structure of the SEI, with a compact inorganic inner layer and a porous organic outer layer.[2,3] However, there is no agreement on which of the two layers actually protects the electrode, even in commercial systems. Early work proposed that growth is limited by electron tunneling or hopping across the compact inorganic layer and was later supported by demonstrations that the inorganic layer forms after the organic layer.[23,24] On the other hand, studies of SEI-forming polymerization reactions have shown correlations between beneficial SEI additives and strong elastic properties of their reduction products, suggesting that organic polymers provide a

Received: July 11, 2018
Revised: August 23, 2018
Published: August 27, 2018

© 2018 American Chemical Society

DOI: 10.1021/acs.jpcc.8b06564
J. Phys. Chem. C 2018, 122, 20632−20641

diffusion barrier to solvent.[25−30] Furthermore, cycle-life studies show that capacity fade scales with $\sqrt{t}$, indicating a transport-limited process that is more consistent with limitations from the porous layer.[31−35]

Accelerated battery failure cannot be resolved without understanding the mechanisms of SEI passivation. However, chemical characterization of SEIs does not identify the property most relevant to battery lifetime: its ability to block electrons. We have previously applied redox mediators as molecular probes of transport and reaction through the SEI.[36−40] In contrast to SEI formation or cation intercalation, the mediator is a fast outer-sphere reaction, so changes to redox mediator kinetics in the presence and absence of SEI can therefore be used to extract quantitative data about charge transport in surface films. Unlike two-electrode coin cell measurements, the mediator method isolates electron from ion transport within the SEI. Extending this method from a rotating disk electrode (RDE) to a rotating ring−disk electrode (RRDE)[41,42] controls electrode crosstalk to intentionally incorporate Mn into the SEI. Additionally, the ability to run collector−generator measurements with the RRDE avoids the need to provide the redox mediator in the oxidized form. As a result, we can systematically vary the electronic and steric properties of the mediator to systematically probe the passivation properties of the SEI. These results reveal a previously unobserved selective transport mechanism. Developing these observations into a coherent model for passivation concludes that the inorganic inner layer is primarily responsible for the SEI's protective behavior.

EXPERIMENTAL SECTION

Electrode Preparation. A solution of $LiNi_{0.5}Mn_{1.5}O_4$ (LNMO) was prepared by suspending 0.1 g of LNMO particles (Sigma-Aldrich) in 10 g of ethanol. The suspension was sonicated for 15 min, and 8 μL of the suspension was drop-casted on the carbon disk of a glassy carbon/glassy carbon RRDE assembly (Pine Instruments). The electrode assembly was dried at room temperature and transferred into an Ar-filled glovebox (LC Technology Solutions) for testing. The dimensions of the ring−disk assembly were 5.61 mm disk outer diameter, 6.25 mm ring inner diameter, 7.92 mm ring outer diameter, 320 μm ring−disk gap, and 15 mm outer diameter PTFE shroud encapsulating the electrodes (Pine Research Instruments). After testing, the ring−disk assembly was removed from the glovebox, gently polished using 1.0 μm alumina MicroPolish (Buehler) on a nylon polishing cloth (BASi), and then sonicated in deionized water for 15 min to remove the alumina particles before drying under vacuum.

Electrochemical Measurements. All electrochemical testing was performed in a custom-made glass cell containing ~12 mL of electrolyte, a Li reference electrode, and a Pt counter electrode. The reference and counter electrodes were separated from the body of the cell by a fritted gas dispersion tube to impede transport of transition metals. Without separation, the Li turned black and the open-circuit voltage drifted significantly, which indicated that transition metals oxidized the reference electrode. The electrolyte was commercial 1 M $LiPF_6$ in ethylene carbonate (EC) and dimethyl carbonate (DMC) (1:1, v:v) (LP 30 Gotion). The redox mediators were introduced to the electrochemical cell in 632 μL additions from a 40 mM stock solution to reach a bulk concentration of ~2 mM.

Prior to adding the redox mediator, the RRDE was rotated at 200 rpm (Pine Research Instruments) in 12 mL of LP 30 electrolyte. The disk was oxidized at a high voltage while the ring cycled from 0.015 to 3 V vs Li/Li+ for three cycles at a scan rate of 20 mV/s. In this potential window, electrolyte reduction and decomposition reactions occurred, and a solid−electrolyte interphase (SEI) was formed on the ring. Then, the redox mediator was added to the electrolyte, and the RRDE rotated at 400 rpm while the open circuit voltage was monitored. Rotation rates were selected to maintain controlled hydrodynamics and steady-state convection, while minimizing undesirable effects of rotation such as shear stress and frictional heating. Once a stable open circuit voltage near the standard redox potential of the added mediator was reached, the disk potential was held at oxidizing limiting current while a CV was performed on the ring, cycling to between −1500 and −1100 mV overpotential. This CV potential window was outside the range of electrolyte reduction, electrolyte oxidation, and SEI oxidation reactions, ensuring that the measured current was attributed solely to redox mediator reactions.

Computational Methods. COMSOL Multiphysics software was used to extract Butler−Volmer rate constants (k_{eff}) and through-film limiting current densities ($i_{lim,f}$) for mediator reduction on the ring electrode for known bulk mediator concentrations and bulk diffusivities. Simulated and experimental $i-V$ curves were compared over a range of k_{eff} and $i_{lim,f}$ input values. A best-fit of k_{eff} and $i_{lim,f}$ for each experimental curve was tabulated.

RESULTS AND DISCUSSION

Mn Contamination of SEI More Disruptive to Through-Film Kinetics than Transport. A schematic representation of how the rotating ring−disk electrode (RRDE) simulates crosstalk from the upstream glassy carbon disk (cathode) to the downstream glassy carbon ring (anode) is shown in Figure 1a. The disk is oxidized at high potential while the ring is cycled to low potential and the entire assembly rotated. Dissolved species then convect to the ring electrode, where they may interact with the formation and

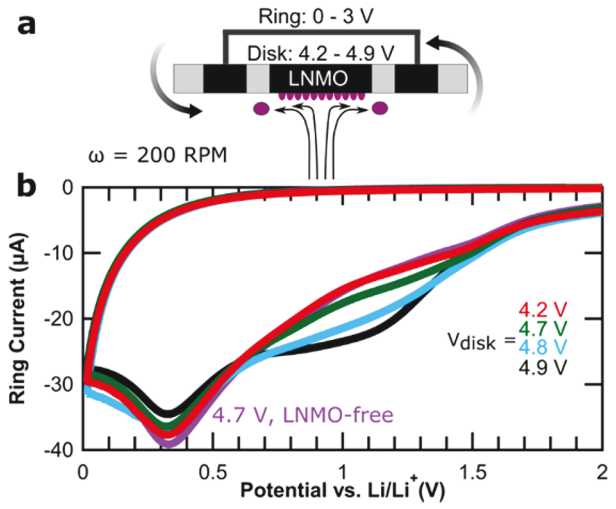

Figure 1. High-voltage LNMO oxidation alters SEI formation via crosstalk. (a) Schematic of RRDE simulating electrode crosstalk and LNMO particle oxidation at disk electrode. (b) First cycle of SEI formation CV on ring downstream from various disk oxidation potentials.

DOI: 10.1021/acs.jpcc.8b06564
J. Phys. Chem. C 2018, 122, 20632−20641

growth of a SEI. Figure 1b demonstrates this effect. In the cyclic voltammogram (CV) of the glassy carbon ring, no Li intercalation is observed at low potentials, consistent with glassy carbon's status as an inert and mechanically robust substrate. When the LNMO-coated disk is held at higher potentials, a new reduction peak near 1.1 V vs Li/Li^+ appears at the ring electrode. The 1.1 V peak may indicate that oxidation products from the disk disrupt the formation of an SEI on the ring or that the oxidation products are electrochemically reduced at this potential. The reduction potentials for Mn^{2+} and Ni^{2+} in nonaqueous electrolyte have not yet been measured, though Komaba reported potentials 1.87 and 2.80 V vs Li/Li^+, respectively, based on standard aqueous redox potentials.[7] Thus, the reduction at 1.1 V vs Li/Li^+ cannot be directly attributed to metal electrodeposition without further investigation of their reduction potentials in nonaqueous electrolyte. The SEI formation CV on the ring appears identical when the disk is held at low potential (4.2 V, red) or when it is LNMO-free (purple), suggesting that 4.2 V oxidation does not result in dissolution, consistent with battery studies.[12,13,43]

After SEI formation on the ring, a redox mediator probes the electrochemical properties of the SEI, as demonstrated in Figure 2a. Potentiostatically holding the disk at the limiting current oxidizes the neutral mediator molecules to their cations, which convect to the passivated ring and are reduced back to the neutral species. Figure 2b displays the cathodic sweeps of CVs at the ring, normalized according to $i_{Norm} = \frac{i_{ring}}{i_{disk} \eta_C}$ for ferrocenium reduction after SEI formation under the various disk conditions in Figure 1b.

The reduction profile with no SEI on the ring is shown in gray for comparison. Without an SEI (gray), the reduction reaction is immeasurably fast, reaching the limiting current around −100 mV overpotential. With a passivating SEI formed in the absence of LNMO (Mn-free, purple), the shallow slope and lack of limiting current demonstrate kinetic and transport barriers to charge transfer. The through-film reduction for SEIs formed downstream of LNMO (contaminated SEI) depends on the oxidation voltage of the disk. At V_{disk} = 4.2 V (red), the through-film ferrocenium reduction is nearly identical to the Mn-free SEI (purple), consistent with battery experiments showing limited capacity fade below 4.3 V.[12,13] As V_{disk} increases above 4.2 V, the contaminated SEI becomes increasingly less passivating with faster reduction kinetics and through-film transport. These observations are consistent with coin-cell studies on the effect of upper cutoff voltage[44] and demonstrate the ability of the approach to reproduce electrode crosstalk. The rapid transport from convection, as well as the ability of the four-electrode system to apply a constant oxidation potential at the disk while varying the reduction potential of the ring, considerably amplifies the effects of Mn dissolution in comparison to a traditional battery. As a result, effects of crosstalk can be observed in minutes, rather than over weeks, of cycling.

In contrast to the electrolyte reduction reactions that form SEI, the mediator reduction is a one-electron outer-sphere electron transfer in supporting electrolyte, which is therefore amenable to traditional electroanalysis.[45] The presence of an SEI results in both kinetic and transport limits to mediator reduction, as represented by the effective kinetic Butler–Volmer rate constant k_{eff} and the through-film limiting current density $i_{lim,f}$, respectively.[36] Both parameters are affected by

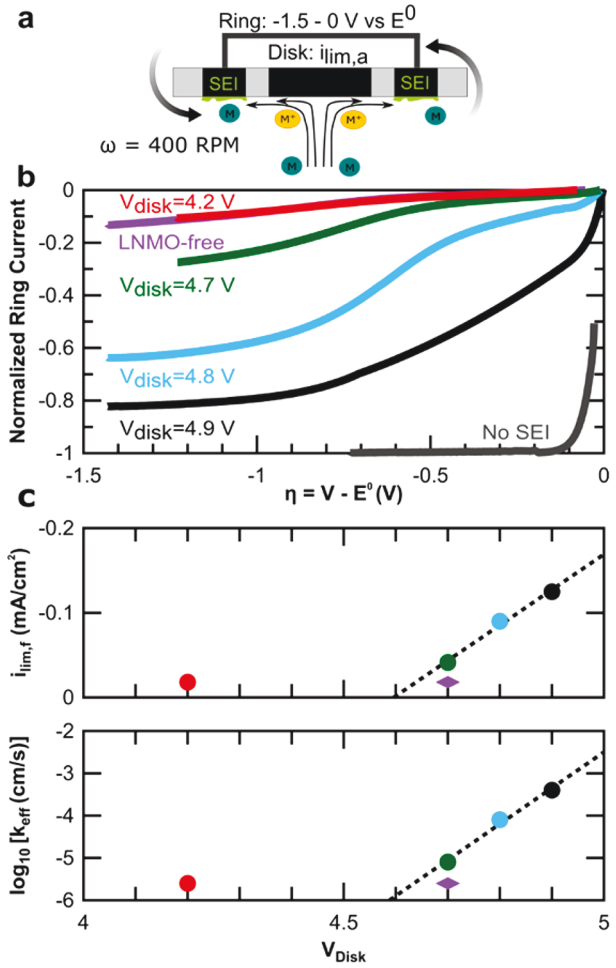

Figure 2. High-voltage Mn dissolution accelerates through-SEI reduction kinetics. (a) Schematic of collector–generator redox mediator method on RRDE. Neutral mediators (blue) oxidize to cations (orange) on the disk and then convect to the ring and reduce back to neutral. (b) CVs for ferrocenium reduction on SEI formed with varying upstream disk conditions. (c) Kinetic and transport parameters of voltammograms via finite element simulations. Dotted line guides the eye for high-voltage experiments with LNMO-coated disk.

morphology and composition of the inner and outer SEI layers, as discussed below.

Because the current distribution on a rotating ring electrode is inherently nonuniform, compared to the rotating disk, finite element simulations were applied to quantitatively interpret the through-film reduction voltammograms. COMSOL was used to simulate solution-phase mediator convection and diffusion, Butler–Volmer ring kinetics, and mediator diffusion through the SEI on the ring. Details are provided in the Supporting Information. The simulated voltammograms were fit to the experimental data to quantify the kinetic and transport parameters k_{eff} and i_{limf} of the through-film reaction (Figure S1). In Figure 2c, these parameters, which correlate inversely with SEI passivity, are plotted against the disk oxidation voltage. The results confirm that increased Mn dissolution at high potential disrupts the SEI's performance. Interestingly, the through-film reduction kinetics are accelerated by orders of magnitude more than the through-film transport. For example, the effective kinetic rate constant through SEI formed with LNMO oxidation at 4.9 V is 160

DOI: 10.1021/acs.jpcc.8b06564
J. Phys. Chem. C 2018, 122, 20632–20641

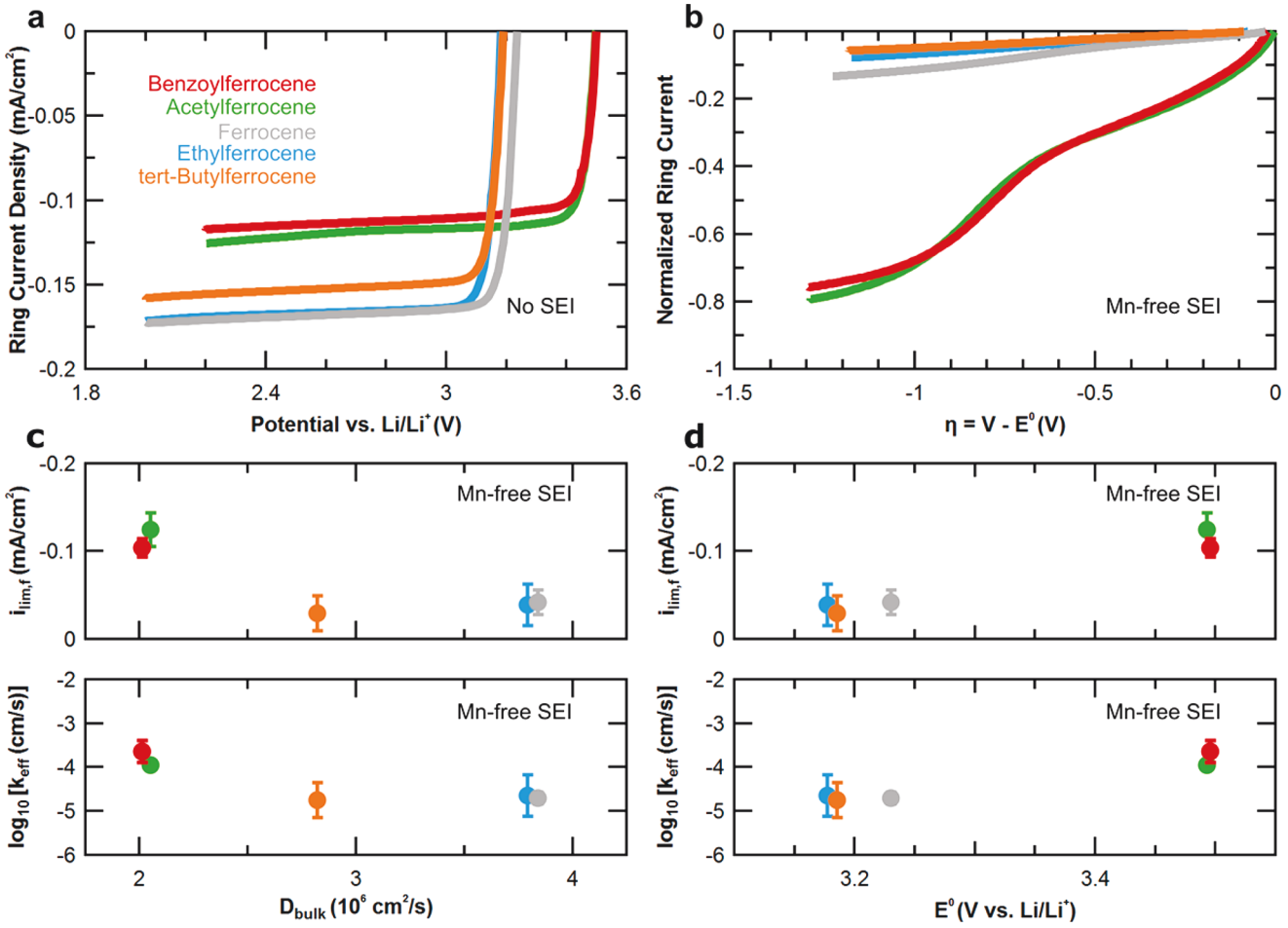

Figure 3. Functionalized redox mediators probe SEI passivation sensitivity. (a) Cyclic voltammograms for mediator reduction on pristine glassy carbon ring electrode. Cathodic sweep shown. (c) Representative cyclic voltammograms for mediator reduction on SEI. Cathodic sweep shown. (c, d) Mean kinetic and transport parameters for mediator cation reduction on Mn-free SEI vs bulk diffusivity (c) and standard potential (d). Error bars represent one standard deviation.

times greater than the rate on the SEI formed in the absence of LNMO, while the through-film limiting current density is only 7 times greater. This discrepancy shows that the presence of transition metals in the SEI has much stronger effects on electronic than morphological properties. However, the ohmic resistance of the SEI remains negligible for all films, including those formed without LNMO (Figure S6).

In addition to the CV SEI formation shown above, constant-current and constant-current−constant-voltage formation procedures were explored. SEIs formed under these protocols were less suitable for this study because they resulted in a completely passivated ring electrode. Accurate resolution of transport and kinetic limits to redox mediator reduction requires moderate through-film electron transfer; thus, fully blocking films cannot be accurately probed by mediator reduction. The CV protocol intentionally grows films which allow some electron transfer so that in situ electrochemical measurements are quickly collected, which would be impossible in coin-cell batteries, and thus the passivation behavior of various films can be distinguished and quantitatively compared.

Functionalized Redox Mediators Show Preferential Reduction in SEI. While the data of Figures 1 and 2 demonstrate the ability to control crosstalk and study effects of Mn contamination on SEI properties, the greater power of the collector−generator approach is the ability to systematically investigate the mechanism of SEI passivation. This is accomplished via functionalization of the redox mediator. Table S1 lists the functionalized ferrocene-based mediators along with selected properties. Representative through-film reduction profiles of the five mediator cations (ferrocenium, ethylferrocenium, *tert*-butylferrocenium, acetylferrocenium, and benzoylferrocenium) are displayed in Figure 3a for a pristine ring and Figure 3b for the SEI formed without upstream LNMO oxidation. There is a clear distinction between the through-film reduction of ferrocenyl alkane mediators (orange, blue, and gray) and ferrocenyl ketone mediators (red and green): reduction of the ferrocenyl ketone cations through the SEI proceeds with faster kinetics and transport. The higher standard redox potentials for the ferrocenyl ketone mediator couples do not explain the observed reduction behavior because plotting current density versus overpotential in Figure 3b accounts for these differences. Additionally, the normalization of the ring current by the disk current and collection efficiency facilitates comparison of mediators with different bulk diffusivities.

The mean effective kinetic rate constants (bottom) and through-film limiting current densities (top) for each mediator on the Mn-free SEI are plotted in Figure 3c with the measured bulk diffusivity (Figure S7) as the abscissa (left) and with the

DOI: 10.1021/acs.jpcc.8b06564
J. Phys. Chem. C 2018, 122, 20632−20641

standard redox potential of the mediator couple as the abscissa (right). The mediator reduction parameters are averaged from finite element simulations of at least four separate experimental trials, with error bars representing one standard deviation from the mean. Figures 3c and 3d show the preferential through-film reduction of ferrocenyl ketones; the effective rate constants are approximately an order of magnitude higher, and the through-film limiting current densities are ~3 times greater than for ferrocenyl alkanes. These parameters do not show a clear trend with either bulk diffusivity or redox potential, indicating that the mechanism by which charge transfer through the SEI is selective for ferrocenyl ketones is due to the polarity of the functional group on the redox mediator, rather than electronegativity or diffusion rate.

Understanding the mechanism of accelerated capacity fade would be incomplete without also investigating how a contaminated SEI fails to passivate the negative electrode. Representative through-film reduction voltammograms of the five mediator cations are displayed in Figure 4 for the SEI

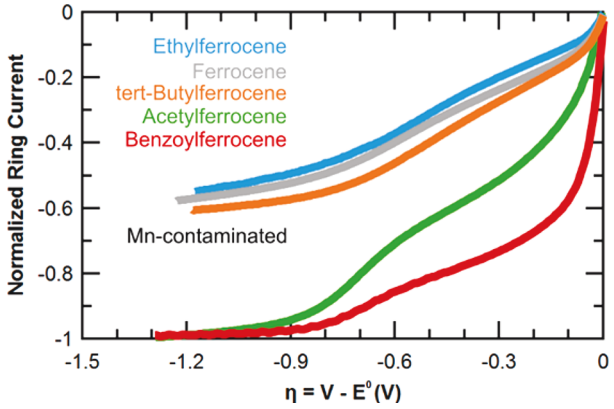

Figure 4. Representative CVs show contaminated SEI is less passivating. Cathodic sweep shown.

contaminated by Mn with V_{disk} = 4.9 V. This high potential ensures maximum effects of electrode crosstalk on the contaminated SEI, as seen in Figure 2c. There is a similar distinction between the reduction of ferrocenyl alkane mediators (orange, blue, and gray) and ferrocenyl ketone mediators (red and green) through the contaminated SEI. Additionally, comparing the voltammograms to those in Figure 3a shows effects of Mn contamination that are consistent with Figure 2b. The normalized reduction current profiles of each mediator through the contaminated SEI shows faster kinetics and through-film transport, indicating diminished passivity of the film.

Corresponding effective kinetic rate constants and through-film limiting current densities determined by finite element simulations for each mediator are shown in Figure 5a against the measured bulk diffusivity and in Figure 5b against the standard redox potential of the mediator couple. Error bars represent one standard deviation from the mean of parameters derived from simulations of at least four experimental trials. Figures 5a and 5b show that, again, there is no clear trend between the effective kinetic rate constant or the through-film limiting current density and the bulk diffusivity or standard redox potential.

Combined, the results of Figures 2–5 show that Mn contamination has a stronger disruptive effect on through-film

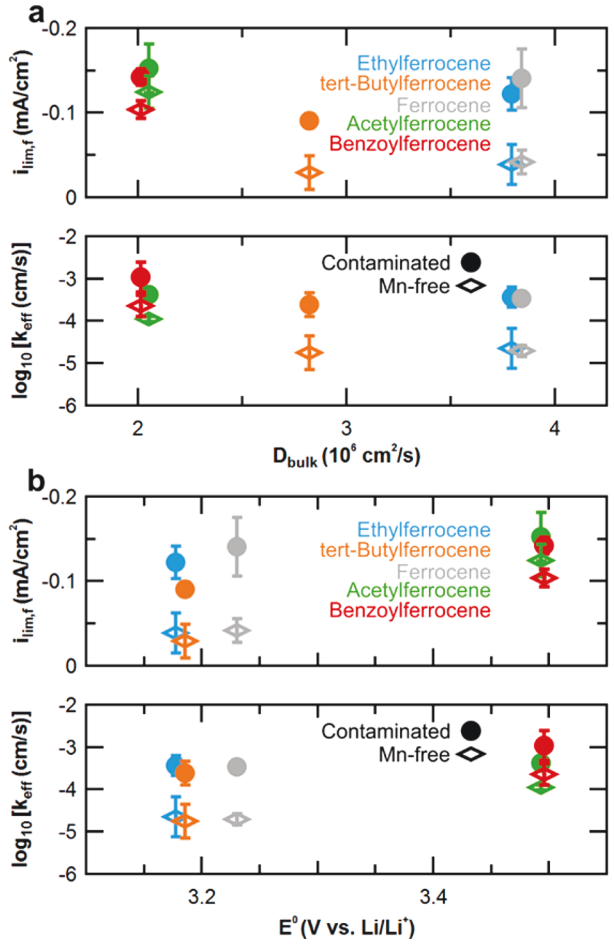

Figure 5. Contaminated SEI allows faster through-film transport and more rapid reduction kinetics (a, b) Mean kinetic and transport parameters found via finite element simulations for mediator cation reduction on contaminated SEI vs bulk diffusivity (a) and standard potential (b). Parameters for Mn-free SEI displayed as diamonds for comparison.

kinetics than on through-film transport and, more surprisingly, that the SEI formed under the same conditions passivates less effectively when the redox mediator contains a ketone group, *even if it is a larger and slower molecule*. This preferential reduction of polar mediators indicates the chemical selectivity of the SEI. Such chemical selectivity, which has not been previously observed, reveals the mechanism by which the SEI protects the electrode. Below, we develop a mechanistic model of SEI formed on carbonaceous anodes that can explain the observations in this work and throughout the literature.

Membrane vs Channel Transport in the Organic SEI Layer. Prospective models for through-film mediator reduction can be implemented from well-established frameworks for mixed kinetics and transport at electroactive films and chemically modified electrodes.[46−51] This field of modified electrodes provides a valuable theoretical and experimental basis for studying passivation and charge transfer but has been historically underutilized in battery literature. Considering the bilayer structure of the SEI, the following cases are specifically considered: (A) channel model for outer layer, (B) electron tunneling across a homogeneous inner layer, (C) membrane model for outer layer, (D) active site model for inner layer, and (E) active site model for Mn-contaminated inner layer. These mechanisms are illustrated in Figure 6. The governing charge-

DOI: 10.1021/acs.jpcc.8b06564
J. Phys. Chem. C 2018, 122, 20632−20641

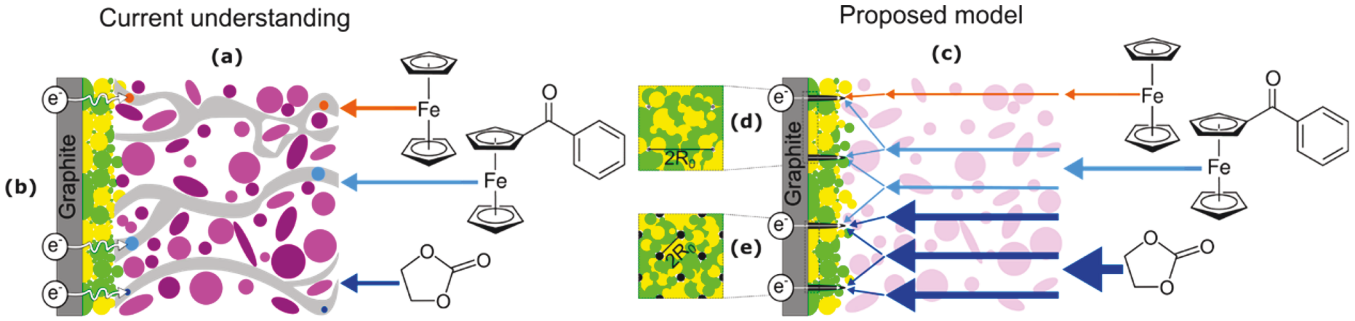

Figure 6. Schematics for proposed mechanistic model contrasted with current understanding of charge transfer through SEI. (a) Channel model of outer SEI layer. (b) Homogenous model of inner SEI layer. (c) Membrane model of outer SEI layer. (d) Active site model of inner SEI layer. (e) Effect of Mn contamination on active site activity and density in the inner SEI layer.

transfer equations under these models are found in Tables S2 and S3.

Conventional understanding of capacity fade considers solvent transport through the outer layer as limited by SEI porosity and tortuosity, while the rate of electron transfer to solvent through the inner layer is limited by electron tunneling.[33,52] Applying this model to the mediator reduction experiments results in a channel diffusion model[53] for the outer layer (Figure 6a) and a macroscopically homogeneous inner layer (Figure 6b). Charge transfer of mediator cations through the outer layer is governed by the bulk diffusivity of the species, $D_{i,\infty}$, and the porosity, ε, tortuosity, τ, and thickness, φ, of the layer.[45] Electron transport through the inner layer is dependent on the thickness of the inner layer,[45] γ, and the porosity of the outer layer, ε, which limits the concentration of oxidized and reduced species reaching the inner layer. Although this model has been used to explain the trend of through-film mediator reduction with the time and potential of SEI formation,[36] it cannot explain the observed kinetic differences between different mediators.

The preferential reduction of ferrocenyl ketone mediators over ferrocenyl alkanes can be explained if the organic outer SEI is considered not as a porous matrix, but rather as a polymer membrane composed of polar organic molecules.[49] In the membrane model, ferrocenyl ketones with slower bulk diffusivity may still have much greater through-film limiting currents due to selective partitioning into the outer SEI layer (Figure 6c). The selective partitioning also leads to higher interfacial concentrations with faster apparent kinetics. This transport mechanism is consistent with current understanding of the chemical composition of the outer layer, which is reported to be composed of alkyl carbonates, oxalates, succinates, and even polymeric species with ethylene oxide and carbonate units.[3] These molecules are likely to have more favorable interactions with ferrocenyl ketones than ferrocenyl alkanes due to the polarity of both species. This results in greater solubility in the outer SEI layer and thus higher concentrations in the film. Consistent with this hypothesis, Kim et al. showed that acetylferrocene was 4 times more soluble than ferrocene in propylene carbonate, a polar solvent.[54]

It is important to distinguish the preferential partitioning of polar vs nonpolar mediators into the SEI from preferential partitioning of polar mediators into SEI vs solvent. Each of the mediators, regardless of polarity, is driven toward the electrode by the concentration gradient formed during reaction. Even if polar mediators have stronger affinity for polar solvent molecules than for polar organic SEI constituents, this affinity is balanced by the concentration gradient at the SEI/electrolyte interface. Thus, polar mediators do not prefer SEI over electrolyte; rather, the SEI prefers polar ferrocenyl ketones to nonpolar ferrocenyl alkanes.

As an alternative explanation, it has recently been demonstrated that the solvation shell of Li greatly influences SEI formation reactions at the anode.[55,56] The preferential coordination of EC to Li has been linked to its increased reactivity compared to linear carbonates.[57,58] However, while Li migration and coordination are important mechanisms for SEI formation, they are unlikely to affect mediator transport in this study. A principal advantage of our technique is operation in supporting electrolyte[59] and at voltages where Li intercalation and electrolyte degradation reactions do not occur. The supporting electrolyte minimizes the impact of migration on mediator transport, unlike Li ions during SEI formation or battery operation. Additionally, without an interfacial Li^+ reaction at the operating voltages, there is no flux of Li ions at the interface and thus no steady-state Li ion migration. Finally, all the mediator cation reduction curves on the pristine electrode in Figure 3a demonstrate similarly Nernstian responses, suggesting that coordination of polar mediators to Li cations has minimal impact on mediator transport. For all these reasons, coordination of mediators to Li cations is inconsistent with the experimental results of this work. Only a preferential affinity of the SEI for polar species can explain the selective reduction observed here.

Active Site Model vs Electron Tunneling. Considering the outer SEI as a solid membrane, rather than a porous medium, accounts for observed selective reduction of ferrocenyl ketones over ferrocenyl alkanes. It remains to interpret the effects of Mn contamination on this mechanism of passivation. Figure 2c shows that Mn contamination affects both kinetics and transport, but the effective kinetic rate constant is accelerated by orders of magnitude more than the through-film limiting current density for all mediators. The hypothesis that Mn contamination leads to a more porous SEI is inconsistent with the membrane model of the outer SEI layer, while changes to the partition coefficient, χ, cannot explain the stronger sensitivity of k_{eff} compared to $i_{lim,f}$.

An alternative to the macroscopically homogeneous inner layer considers a series of pinholes or active sites[47] in an otherwise impermeable matrix (Figure 6d, e). The active site model is consistent with theoretical predictions of anomalous conduction at grain boundaries[60,61] and experimental observations of microscopic defects in the SEI,[62] both of which may function as active sites. This model introduces a kinetic dependence on the active site density, $1 - \theta$, which also affects

DOI: 10.1021/acs.jpcc.8b06564
J. Phys. Chem. C 2018, 122, 20632−20641

the through-film limiting current density. Therefore, the Mn-contaminated SEI (Figure 6e), relative to the Mn-free SEI (Figure 6d), has a higher fractional coverage of active sites, and these active sites are closer together, resulting in faster through-film transport. These Mn-generated active sites are also "more active" than those present in the Mn-free SEI. The effective rate constant increases exponentially with Mn contamination (Figure 2b) because Mn lowers the barrier for electron transfer to SEI species at the inner/outer SEI layer interface.[13,20,21] A lower barrier at the Mn-containing active sites manifests in this model as a higher electron-transfer rate constant, k_0 (Table S2), and could be caused if electronic states from Mn dopants decrease the band gap of normally insulating SEI species.[63] Ultimately, the increased activity of active sites greatly diminishes the barrier for electron transfer to bulk electrolyte molecules, while the increased density of active sites shortens the two-dimensional diffusion length of reactive species. The result is additional and continual electrolyte reduction leading to severe capacity fade.

The experimental findings and proposed mechanistic model in this work do not support the hypothesis that Mn clusters form a conductive pathway for electrons from the negative electrode to the bulk electrolyte. If this were the case, electron transfer to the redox mediators would be rapid, inconsistent with experimental observations of kinetic barriers to electron transfer even in a contaminated film. An electron-conducting SEI also fails to account for observed chemical selectivity. A final piece of evidence against an electron-conducting mechanism is the nonlinear $i-V$ curves for mediator reduction and the low impedance of both Mn-contaminated and Mn-free SEIs (Figure S6). Additionally, the hypothesis that Mn accelerates capacity fade via cracks in the outer layer is not supported by this work because simply considering the outer layer as a series of cracks or channels through which solvent diffuses cannot account for the chemical selectivity observed in this study. Experimental observations and the proposed model agree with the mechanisms proposed by several groups that Mn dispersed either within the inner layer or on the surface of the inner layer reduces the barrier of electron transfer by forming catalytic active sites.[13,14,20,21]

Although the experiments yielding these findings were performed on nonintercalating glassy carbon electrodes, the implications for current understanding of the SEI extend to graphite and other practical carbonaceous anodes. Glassy carbon is often employed as a model electrode for graphite when porosity is detrimental to analytical techniques,[64] and the lack of lithium intercalation into glassy carbon prevents issues of volume expansion and associated mechanical stresses enabling investigation by SECM and RDE/RRDE.[42,65] Two groups independently demonstrated that the composition and behavior of SEIs formed on glassy carbon are comparable to those formed on both the basal plane of graphite and on disordered hard carbons.[66−69] Novak and co-workers also confirmed the similarity of the two carbon electrode types with respect to both ethylene evolution and infrared spectroscopy.[68,69] Additionally, McCreery's group used Raman spectroscopy and electrochemistry to show that graphite edge planes within glassy carbon were the active sites for electron transfer.[70] Peled and colleagues used XPS and TOFSIMS to study SEI composition on various carbons and showed that SEI on hard carbons, like glassy carbon, is most similar to SEI on the cross section of HOPG, in which there is lithium intercalation.[67] Despite the lack of lithium intercalation, there is overwhelming evidence that SEIs formed on glassy carbon are indeed highly similar to those formed on graphite.

Implications for Battery Lifetime and Interface Design. Only a model combining an active-site inner SEI layer and membrane-like outer SEI layer is fully consistent with the findings in this work and in the literature. A schematic representation of this model can be found in Figure 6. Transport in the outer layer is governed by the partition coefficient at the solution−film interface, χ, the effective diffusivity in the film, $D_{i,f}$, and the thickness of the outer SEI layer, φ, while diffusion from the outer layer/inner layer interface to active sites is dependent on active site density, $1-\theta$, distance between active sites, $2R_0$, and the species diffusivity in the film, $D_{i,f}$. Kinetics in the interphase are governed by partition coefficients, the active site density, and the rate of electron transfer at the active sites, k_0. In this model, Mn aggressively disrupts the inner layer of the SEI in its role of protecting the electrolyte from continual reduction by simultaneously increasing the activity (k_0) and density ($1-\theta$) of active sites (Figure 6e).

The most important implication of the model proposed in this work is the conclusion that the inner layer, rather than the outer layer, is responsible for protecting the electrolyte from the carbon electrode. This conclusion can be reached by considering the nature of the SEI's chemical selectivity. If the organic outer SEI layer is selectively permeable to molecules with polar ketone groups, it stands to reason that both linear and cyclic carbonates should be even more soluble than the ferrocenyl ketones in our study due to their similar chemical functionality, higher polarity, and smaller size. Considering the undeniable role of carbonate reduction in SEI formation and capacity fade, we conclude that *the outer SEI layer does not pose significant barriers to solvent diffusion*. Rather, the inner layer critically protects the electrolyte from continual reduction at the negative electrode because it is electronically insulating with an extremely low density of defects or active sites. Under this mechanism, electrolyte reduction is limited by low availability of active sites for reduction, and two-dimensional diffusion across the inner layer surface to the active sites results in the commonly observed $\sqrt{t}$ dependence of capacity fade.

CONCLUSIONS

In summary, a generator−collector methodology developed around redox mediators as molecular probes has been used to reveal the previously unobserved chemical selectivity of the SEI. This selectivity strongly suggests that the inner inorganic SEI layer provides the critical components of passivation in Li-ion batteries, while the outer organic layer plays a minimal role at best. The resulting model of a membrane-like outer SEI layer and active-site inner layer is consistent with experimental observations of SEI passivation on an RRDE as well as Mn-induced capacity fade. This new understanding of the SEI has two critical consequences for interface design in both established Li-ion and novel "beyond Li" systems. First, it suggests that characterization of battery interfaces should focus on the role of inorganic components like Li_2CO_3 and LiF rather than the polymers which make up the majority of the SEI volume, especially when determining the effects of electrolyte additives. Second, efforts to develop an "artificial SEI"[71] based on organic protection layers are inherently less likely to succeed than inorganic protection layers. In particular, our model suggests that the dense, cross-linked polymers formed by the well-known additives FEC and VC are

DOI: 10.1021/acs.jpcc.8b06564
J. Phys. Chem. C 2018, 122, 20632−20641

passivating not because of the polymers themselves but because of the increased ease of mineralizing the polymer layer to inorganics.[29,30,72] Ultimately, better understanding of interfacial transport and reaction will lead to new approaches for preventing accelerated capacity fade in high-voltage batteries as well as targeted interfacial design of the negative electrode for many beyond-Li systems.

■ ASSOCIATED CONTENT

Supporting Information

The Supporting Information is available free of charge on the ACS Publications website at DOI: 10.1021/acs.jpcc.8b06564.

Finite element simulation parameter selection and model validation; electrochemical impedance spectra for contaminated SEI, Mn-free SEI, and pristine electrode; measured electrochemical and transport properties of the redox mediators; and development of mechanistic models for SEI passivation (PDF)

■ AUTHOR INFORMATION

Corresponding Author

*E-mail mhtang@drexel.edu (M.H.T.).

ORCID

Oliver C. Harris: 0000-0002-5484-5688

Maureen H. Tang: 0000-0003-0037-4814

Notes

The authors declare no competing financial interest.

■ ACKNOWLEDGMENTS

This work was supported by NSF- 820134.

■ REFERENCES

(1) Peled, E. The Electrochemical-Behavior of Alkali and Alkaline-Earth Metals in Non-Aqueous Battery Systems - the Solid Electrolyte Interphase Model. *J. Electrochem. Soc.* **1979**, *126*, 2047−2051.

(2) Xu, K. Nonaqueous Liquid Electrolytes for Lithium-Based Rechargeable Batteries. *Chem. Rev.* **2004**, *104*, 4303−4417.

(3) Xu, K. Electrolytes and Interphases in Li-Ion Batteries and Beyond. *Chem. Rev.* **2014**, *114*, 11503−11618.

(4) Abraham, D. P.; Spila, T.; Furczon, M. M.; Sammann, E. Evidence of Transition-Metal Accumulation on Aged Graphite Anodes by SIMS. *Electrochem. Solid-State Lett.* **2008**, *11*, A226.

(5) Zhan, C.; Lu, J.; Jeremy Kropf, A.; Wu, T.; Jansen, A. N.; Sun, Y.-K.; Qiu, X.; Amine, K. Mn(II) Deposition on Anodes and Its Effects on Capacity Fade in Spinel Lithium Manganate−carbon Systems. *Nat. Commun.* **2013**, *4*, 2437.

(6) Li, Y.; Bettge, M.; Polzin, B.; Zhu, Y.; Balasubramanian, M.; Abraham, D. P. Understanding Long-Term Cycling Performance of Li1.2Ni0.15Mn0.55Co0.1O2−Graphite Lithium-Ion Cells. *J. Electrochem. Soc.* **2013**, *160*, A3006−A3019.

(7) Komaba, S.; Kumagai, N.; Kataoka, Y. Influence of Manganese(II), Cobalt(II), and Nickel(II) Additives in Electrolyte on Performance of Graphite Anode for Lithium-Ion Batteries. *Electrochim. Acta* **2002**, *47*, 1229−1239.

(8) Tsunekawa, H.; Tanimoto, S.; Marubayashi, R.; Fujita, M.; Kifune, K.; Sano, M. Capacity Fading of Graphite Electrodes Due to the Deposition of Manganese Ions on Them in Li-Ion Batteries. *J. Electrochem. Soc.* **2002**, *149*, A1326.

(9) Lu, D.; Xu, M.; Zhou, L.; Garsuch, A.; Lucht, B. L. Failure Mechanism of Graphite/LiNi0.5Mn1.5O4 Cells at High Voltage and Elevated Temperature. *J. Electrochem. Soc.* **2013**, *160*, A3138−A3143.

(10) Ochida, M.; Domi, Y.; Doi, T.; Tsubouchi, S.; Nakagawa, H.; Yamanaka, T.; Abe, T.; Ogumi, Z. Influence of Manganese Dissolution on the Degradation of Surface Films on Edge Plane Graphite Negative-Electrodes in Lithium-Ion Batteries. *J. Electrochem. Soc.* **2012**, *159*, A961−A966.

(11) Jang, D. H.; Shin, Y. J.; Oh, S. M. Dissolution of Spinel Oxides and Capacily Losses in 4 V. *J. Electrochem. Soc.* **1996**, *143*, 2204−2211.

(12) Jarry, A.; Gottis, S.; Yu, Y.-S.; Roque-Rosell, J.; Kim, C.; Cabana, J.; Kerr, J.; Kostecki, R. The Formation Mechanism of Fluorescent Metal Complexes at the Li x Ni 0.5 Mn 1.5 O 4−δ /Carbonate Ester Electrolyte Interface. *J. Am. Chem. Soc.* **2015**, *137*, 3533−3539.

(13) Gilbert, J. A.; Shkrob, I. A.; Abraham, D. P. Transition Metal Dissolution, Ion Migration, Electrocatalytic Reduction and Capacity Loss in Lithium-Ion Full Cells. *J. Electrochem. Soc.* **2017**, *164*, A389−A399.

(14) Gowda, S. R.; Gallagher, K. G.; Croy, J. R.; Bettge, M.; Thackeray, M. M.; Balasubramanian, M. Oxidation State of Cross-over Manganese Species on the Graphite Electrode of Lithium-Ion Cells. *Phys. Chem. Chem. Phys.* **2014**, *16*, 6898−6902.

(15) Pieczonka, N. P. W.; Liu, Z.; Lu, P.; Olson, K. L.; Moote, J.; Powell, B. R.; Kim, J. Understanding Transition-Metal Dissolution Behavior in LiNi 0.5 Mn 1.5 O 4 High-Voltage Spinel for Lithium Ion Batteries. *J. Phys. Chem. C* **2013**, *117*, 15947−15957.

(16) Tsujikawa, T.; Yabuta, K.; Matsushita, T.; Arakawa, M.; Hayashi, K. A Study on the Cause of Deterioration in Float-Charged Lithium-Ion Batteries Using LiMn[Sub 2]O[Sub 4] as a Cathode Active Material. *J. Electrochem. Soc.* **2011**, *158*, A322.

(17) Xiao, X.; Liu, Z.; Baggetto, L.; Veith, G. M.; More, K. L.; Unocic, R. R. Unraveling Manganese Dissolution/Deposition Mechanisms on the Negative Electrode in Lithium Ion Batteries. *Phys. Chem. Chem. Phys.* **2014**, *16*, 10398−10402.

(18) Delacourt, C.; Kwong, A.; Liu, X.; Qiao, R.; Yang, W. L.; Lu, P.; Harris, S. J.; Srinivasan, V. Effect of Manganese Contamination on the Solid-Electrolyte-Interphase Properties in Li-Ion Batteries. *J. Electrochem. Soc.* **2013**, *160*, A1099−A1107.

(19) Joshi, T.; Eom, K.; Yushin, G.; Fuller, T. F. Effects of Dissolved Transition Metals on the Electrochemical Performance and SEI Growth in Lithium-Ion Batteries. *J. Electrochem. Soc.* **2014**, *161*, A1915−A1921.

(20) Shkrob, I. A.; Kropf, a. J.; Marin, T. W.; Li, Y.; Poluektov, O. G.; Niklas, J.; Abraham, D. P. Manganese in Graphite Anode and Capacity Fade in Li Ion Batteries. *J. Phys. Chem. C* **2014**, *118*, 24335−24348.

(21) Vissers, D. R.; Chen, Z.; Shao, Y.; Engelhard, M. H.; Das, U.; Redfern, P. C.; Curtiss, L. A.; Pan, B.; Liu, J.; Amine, K. Role of Manganese Deposition on Graphite in the Capacity Fading of Lithium Ion Batteries. *ACS Appl. Mater. Interfaces* **2016**, *8*, 14244−14251.

(22) Leung, K. First-Principles Modeling of Mn(II) Migration above and Dissolution from Li $_x$ Mn $_2$ O $_4$ (001) Surfaces. *Chem. Mater.* **2017**, *29*, 2550−2562.

(23) Lu, P.; Harris, S. J. Lithium Transport within the Solid Electrolyte Interphase. *Electrochem. Commun.* **2011**, *13*, 1035−1037.

(24) Lu, P.; Li, C.; Schneider, E. W.; Harris, S. J. Chemistry, Impedance, and Morphology Evolution in Solid Electrolyte Interphase Films during Formation in Lithium Ion Batteries. *J. Phys. Chem. C* **2014**, *118*, 896−903.

(25) Su, X.; Wu, Q.; Li, J.; Xiao, X.; Lott, A.; Lu, W.; Sheldon, B. W.; Wu, J. Silicon-Based Nanomaterials for Lithium-Ion Batteries: A Review. *Adv. Energy Mater.* **2014**, *4*, 1300882.

(26) Nguyen, C. C.; Lucht, B. L. Comparative Study of Fluoroethylene Carbonate and Vinylene Carbonate for Silicon Anodes in Lithium Ion Batteries. *J. Electrochem. Soc.* **2014**, *161*, A1933−A1938.

(27) Takenaka, N.; Suzuki, Y.; Sakai, H.; Nagaoka, M. On Electrolyte-Dependent Formation of Solid Electrolyte Interphase Film in Lithium-Ion Batteries: Strong Sensitivity to Small Structural Difference of Electrolyte Molecules. *J. Phys. Chem. C* **2014**, *118*, 10874−10882.

(28) Madec, L.; Petibon, R.; Tasaki, K.; Xia, J.; Sun, J. P.; Hill, I. G.; Dahn, J. R. Mechanism of Action of Ethylene Sulfite and Vinylene Carbonate Electrolyte Additives in LiNi1/3Mn1/3Co1/3O2/Graphite Pouch Cells: Electrochemical, GC-MS and XPS Analysis. *Phys. Chem. Chem. Phys.* **2015**, *17*, 27062−27076.
(29) Shkrob, I. A.; Wishart, J. F.; Abraham, D. P. What Makes Fluoroethylene Carbonate Different? *J. Phys. Chem. C* **2015**, *119*, 14954−14964.
(30) Jin, Y.; Kneusels, N. J. H.; Magusin, P. C. M. M.; Kim, G.; Castillo-Martínez, E.; Marbella, L. E.; Kerber, R. N.; Howe, D. J.; Paul, S.; Liu, T.; et al. Identifying the Structural Basis for the Increased Stability of the Solid Electrolyte Interphase Formed on Silicon with the Additive Fluoroethylene Carbonate. *J. Am. Chem. Soc.* **2017**, *139*, 14992−15004.
(31) Broussely, M.; Herreyre, S.; Biensan, P.; Kasztejna, P.; Nechev, K.; Staniewicz, R. J. Aging Mechanism in Li Ion Cells and Calendar Life Predictions. *J. Power Sources* **2001**, *97*−*98*, 13−21.
(32) Ploehn, H. J.; Ramadass, P.; White, R. E. Solvent Diffusion Model for Aging of Lithium-Ion Battery Cells. *J. Electrochem. Soc.* **2004**, *151*, A456.
(33) Safari, M.; Morcrette, M.; Teyssot, A.; Delacourt, C. Multimodal Physics-Based Aging Model for Life Prediction of Li-Ion Batteries. *J. Electrochem. Soc.* **2009**, *156*, A145.
(34) Pinson, M. B.; Bazant, M. Z. Theory of SEI Formation in Rechargeable Batteries: Capacity Fade, Accelerated Aging and Lifetime Prediction. *J. Electrochem. Soc.* **2013**, *160*, A243−A250.
(35) Hao, F.; Liu, Z.; Balbuena, P. B.; Mukherjee, P. P. Mesoscale Elucidation of Solid Electrolyte Interphase Layer Formation in Li-Ion Battery Anode. *J. Phys. Chem. C* **2017**, *121*, 26233−26240.
(36) Tang, M.; Newman, J. Electrochemical Characterization of SEI-Type Passivating Films Using Redox Shuttles. *J. Electrochem. Soc.* **2011**, *158*, A530.
(37) Tang, M.; Miyazaki, K.; Abe, T.; Newman, J. Effect of Graphite Orientation and Lithium Salt on Electronic Passivation of Highly Oriented Pyrolytic Graphite. *J. Electrochem. Soc.* **2012**, *159*, A634.
(38) Tang, M.; Newman, J. Transient Characterization of Solid-Electrolyte-Interphase Using Ferrocene. *J. Electrochem. Soc.* **2012**, *159*, A281.
(39) Tang, M.; Lu, S.; Newman, J. Experimental and Theoretical Investigation of Solid-Electrolyte-Interphase Formation Mechanisms on Glassy Carbon. *J. Electrochem. Soc.* **2012**, *159*, A1775−A1785.
(40) Tang, M.; Newman, J. Why Is the Solid-Electrolyte-Interphase Selective? Through-Film Ferrocenium Reduction on Highly Oriented Pyrolytic Graphite. *J. Electrochem. Soc.* **2012**, *159*, A1922−A1927.
(41) Wang, L.-F.; Ou, C.-C.; Striebel, K. A.; Chen, J.-S. Study of Mn Dissolution from LiMn[Sub 2]O[Sub 4] Spinel Electrodes Using Rotating Ring-Disk Collection Experiments. *J. Electrochem. Soc.* **2003**, *150*, A905.
(42) Kaymaksiz, S.; Wachtler, M.; Wohlfahrt-Mehrens, M. Influence of the Solid Electrolyte Interphase on the Performance of Redox Shuttle Additives in Li-Ion Batteries - A Rotating Ring-Disc Electrode Study. *J. Power Sources* **2015**, *273*, 123−127.
(43) Zheng, H.; Sun, Q.; Liu, G.; Song, X.; Battaglia, V. S. Correlation between Dissolution Behavior and Electrochemical Cycling Performance for LiNi1/3Co1/3Mn1/3O2-Based Cells. *J. Power Sources* **2012**, *207*, 134−140.
(44) Gilbert, J. A.; Bareño, J.; Spila, T.; Trask, S. E.; Miller, D. J.; Polzin, B. J.; Jansen, A. N.; Abraham, D. P. Cycling Behavior of NCM523/Graphite Lithium-Ion Cells in the 3−4.4 V Range: Diagnostic Studies of Full Cells and Harvested Electrodes. *J. Electrochem. Soc.* **2017**, *164*, A6054−A6065.
(45) Bard, A. J.; Faulkner, L. R. *Electrochemical Methods Fundamentals and Applications*, 2nd ed.; Wiley: New York, 2001.
(46) Gueshi, T.; Tokuda, K.; Matsuda, H. Voltammetry at Partially Covered Electrodes: Part I. Chronopotentiometry and Chronoamperometry at Model Electrodes. *J. Electroanal. Chem. Interfacial Electrochem.* **1978**, *89*, 247−260.
(47) Gueshi, T.; Tokuda, K.; Matsuda, H. Voltammetry at Partially Covered Electrodes: Part II. Linear Potential Sweep and Cyclic Voltammetry. *J. Electroanal. Chem. Interfacial Electrochem.* **1979**, *101*, 29−38.
(48) Peerce, P. J.; Bard, A. J. Polymer Films on Electrodes. Part II. Film Structure and Mechanism of Electron Transfer with Electrodeposited Poly(Vinylferrocene). *J. Electroanal. Chem. Interfacial Electrochem.* **1980**, *112*, 97−115.
(49) Leddy, J.; Bard, A. J. Polymer Films on Electrodes. Part XII. Chronoamperometric and Rotating Disk Electrode Determination of the Mechanism of Mass Transport through Poly(Vinyl Ferrocene) Films. *J. Electroanal. Chem. Interfacial Electrochem.* **1983**, *153*, 223−242.
(50) Amatore, C.; Savéant, J. M.; Tessier, D. Charge Transfer at Partially Blocked Surfaces. A Model for the Case of Microscopic Active and Inactive Sites. *J. Electroanal. Chem. Interfacial Electrochem.* **1983**, *147*, 39−51.
(51) Leddy, J.; Bard, A. J.; Maloy, J. T.; Savéant, J. M. Kinetics of Film-Coated Electrodes. *J. Electroanal. Chem. Interfacial Electrochem.* **1985**, *187*, 205−227.
(52) Li, D.; Danilov, D.; Zhang, Z.; Chen, H.; Yang, Y.; Notten, P. H. L. Modeling the SEI-Formation on Graphite Electrodes in LiFePO4 Batteries. *J. Electrochem. Soc.* **2015**, *162*, A858−A869.
(53) Saveant, J.-M. Permeation Membrane through Polymer Coatings on Electrodes versus Pinhole Permeation. *J. Electroanal. Chem. Interfacial Electrochem.* **1991**, *302*, 91−101.
(54) Kim, H. S.; Yoon, T.; Kim, Y.; Hwang, S.; Ryu, J. H.; Oh, S. M. Increase of Both Solubility and Working Voltage by Acetyl Substitution on Ferrocene for Non-Aqueous Flow Battery. *Electrochem. Commun.* **2016**, *69*, 72−75.
(55) Xu, K.; Von Wald Cresce, A. Li+-Solvation/Desolvation Dictates Interphasial Processes on Graphitic Anode in Li Ion Cells. *J. Mater. Res.* **2012**, *27*, 2327−2341.
(56) Xing, L.; Zheng, X.; Schroeder, M.; Alvarado, J.; von Wald Cresce, A.; Xu, K.; Li, Q.; Li, W. Deciphering the Ethylene Carbonate−Propylene Carbonate Mystery in Li-Ion Batteries. *Acc. Chem. Res.* **2018**, *51*, 282.
(57) Jeong, S.-K.; Inaba, M.; Iriyama, Y.; Abe, T.; Ogumi, Z. Surface Film Formation on a Graphite Negative Electrode in Lithium-Ion Batteries: AFM Study on the Effects of Co-Solvents in Ethylene Carbonate-Based Solutions. *Electrochim. Acta* **2002**, *47*, 1975−1982.
(58) Wang, Y.; Balbuena, P. B. Theoretical Studies on Cosolvation of Li Ion and Solvent Reductive Decomposition in Binary Mixtures of Aliphatic Carbonates. *Int. J. Quantum Chem.* **2005**, *102*, 724−733.
(59) Newman, J.; Thomas-Alyea, K. *Electrochemical Systems*, 3rd ed.; Wiley: New York, 2004.
(60) Leung, K.; Jungjohann, K. L. Spatial Heterogeneities and Onset of Passivation Breakdown at Lithium Anode Interfaces. *J. Phys. Chem. C* **2017**, *121*, 20188−20196.
(61) Zhang, Q.; Pan, J.; Lu, P.; Liu, Z.; Verbrugge, M. W.; Sheldon, B. W.; Cheng, Y. T.; Qi, Y.; Xiao, X. Synergetic Effects of Inorganic Components in Solid Electrolyte Interphase on High Cycle Efficiency of Lithium Ion Batteries. *Nano Lett.* **2016**, *16*, 2011−2016.
(62) Li, Y.; Li, Y.; Pei, A.; Yan, K.; Sun, Y.; Wu, C.-L.; Joubert, L.-M.; Chin, R.; Koh, A. L.; Yu, Y.; et al. Atomic Structure of Sensitive Battery Materials and Interfaces Revealed by Cryo−electron Microscopy. *Science (Washington, DC, U. S.)* **2017**, *358*, 506−510.
(63) Lin, Y. X.; Liu, Z.; Leung, K.; Chen, L. Q.; Lu, P.; Qi, Y. Connecting the Irreversible Capacity Loss in Li-Ion Batteries with the Electronic Insulating Properties of Solid Electrolyte Interphase (SEI) Components. *J. Power Sources* **2016**, *309*, 221−230.
(64) Pérez-Villar, S.; Lanz, P.; Schneider, H.; Novák, P. Characterization of a Model Solid Electrolyte Interphase/Carbon Interface by Combined in Situ Raman/Fourier Transform Infrared Microscopy. *Electrochim. Acta* **2013**, *106*, 506−515.
(65) Zampardi, G.; La Mantia, F.; Schuhmann, W. Determination of the Formation and Range of Stability of the SEI on Glassy Carbon by Local Electrochemistry. *RSC Adv.* **2015**, *5*, 31166−31171.
(66) Peled, E.; Bar Tow, D.; Merson, A.; Gladkich, A.; Burstein, L.; Golodnitsky, D. Composition, Depth Profiles and Lateral Distribution

DOI: 10.1021/acs.jpcc.8b06564
J. Phys. Chem. C 2018, 122, 20632−20641

of Materials in the SEI Built on HOPG-TOF SIMS and XPS Studies. *J. Power Sources* **2001**, *97*−*98*, 52−57.
(67) Peled, E.; Golodnitsky, D.; Ulus, A.; Yufit, V. Effect of Carbon Substrate on SEI Composition and Morphology. *Electrochim. Acta* **2004**, *50*, 391−395.
(68) Imhof, R.; Novák, P. In Situ Investigation of the Electrochemical Reduction of Carbonate Electrolyte Solutions at Graphite Electrodes. *J. Electrochem. Soc.* **1998**, *145*, 1081.
(69) Novák, P.; Joho, F.; Imhof, R.; Panitz, J.-C.; Haas, O. In Situ Investigation of the Interaction between Graphite and Electrolyte Solutions. *J. Power Sources* **1999**, *81*−*82*, 212−216.
(70) Rice, R. J.; Pontikos, N. M.; McCreery, R. L. Quantitative Correlations of Heterogeneous Electron-Transfer Kinetics with Surface Properties of Glassy Carbon Electrodes. *J. Am. Chem. Soc.* **1990**, *112*, 4617−4622.
(71) Tu, Z.; Choudhury, S.; Zachman, M. J.; Wei, S.; Zhang, K.; Kourkoutis, L. F.; Archer, L. A. Designing Artificial Solid-Electrolyte Interphases for Single-Ion and High-Efficiency Transport in Batteries. *Joule* **2017**, *1*, 394−406.
(72) Soto, F. A.; Ma, Y.; Martinez de la Hoz, J. M.; Seminario, J. M.; Balbuena, P. B. Formation and Growth Mechanisms of Solid-Electrolyte Interphase Layers in Rechargeable Batteries. *Chem. Mater.* **2015**, *27*, 7990−8000.

DOI: 10.1021/acs.jpcc.8b06564
J. Phys. Chem. C 2018, 122, 20632−20641